Chapter 2
AGN: Absorption, Spectral Classification and the Optical Emission Lines

Scientific theory is a contrived foothold in the chaos of living phenomena.

Wilhelm Reich (1897–1957)

2.1 Synopsis

In this chapter I examine the properties of a sample of nearby galaxies through the use of an archival *Chandra* snapshot survey, with particular emphasis on absorption and the identification of Compton-thick sources. I also discuss the importance of the optical emission lines and, in particular, their use in distinguishing direct AGN emission from starburst emission or reprocessed emission from obscured sources. Although this chapter arises from a separate body of work from that described in later chapters, the results are nevertheless relevant to the selection of AGN sources in Chap. 4. In addition, the distribution of Γ with respect to $\dot{m}_{\mathrm{E}}$ within this sample (which is discussed at the beginning of Chap. 4) leads naturally to my examination in Chaps. 3 and 4 of how this relationship evolves within individual sources.

2.2 Introduction

Active galactic nuclei (AGN) are widely believed to be powered by accretion onto supermassive black holes (SMBHs), and it is therefore natural to expect that their behaviour should, at least to some extent, mirror that of Galactic X-ray binary systems (XRBs). However, the galactic nuclei in which AGN lie are likely to have very different properties from the local environments of Galactic XRBs, with a much greater density of surrounding matter and therefore an increased risk of contamination from nearby sources.

C. Skipper, *Fast Spectral Variability in the X-ray Emission of Accreting Black Holes*, Springer Theses, DOI 10.1007/978-3-319-09587-5_2

Observationally, AGN are divided into several different types depending upon their properties, and some types are further divided into several sub-types. For example, sources from which broad emission lines have been detected are classified as either type 1.0, 1.2, 1.5, 1.8, 1.9 or 2.0 (Osterbrock 1977), depending upon the strength of the H α and H β lines. It has been suggested (e.g. Antonucci and Miller 1985) that these different classes can be unified within a single scenario in which the orientation of the system with respect to the observer is the main factor in producing the different observed properties. The original proposal for a unified scheme was based upon the discovery of polarised broad lines in the optical spectrum of the Seyfert-2 galaxy NGC 1068 and, since then, polarised broad lines have been discovered in $\sim$50 % of Seyfert-2 galaxies for which we have suitable spectropolarimetric data (Tran 2001). However, in recent years a number of sources have been identified that appear to be inconsistent with the unified model (e.g. Pappa et al. 2001; Panessa and Bassani 2002; Georgantopoulos and Zezas 2003; Bianchi et al. 2008) and, in particular, very little is known about the degree to which the unified model applies to low luminosity AGN (LLAGN).

In order to compare the behaviour of AGN to that of XRBs it is therefore crucial that we understand the nature of the objects that we are studying. For instance, it has been suggested that low-ionisation nuclear emission line regions (LINERs) are the AGN equivalent of hard-state Galactic XRBs (e.g. Narayan and McClintock 2008; Constantin et al. 2009; Younes et al. 2011), and should therefore be described using a radiatively inefficient accretion flow (RIAF) model (Narayan et al. 1998; Quataert 2001). Another potential source of confusion when studying AGN is the degree of absorption affecting our view of the source, and recognising the difference between AGN emission that is unabsorbed and emission that is reprocessed (by reflection or scattering, for example) has often proved more difficult than one would imagine.

The majority of nearby galaxies are classified as having H II region nuclei, and it is expected that star formation is likely to play a significant role in most (if not all) of their properties. H II region galaxies are almost always late-type spirals with relatively small black hole masses ($M_{\rm BH} \le 10^7 M_\odot$) and few of these sources contain unresolved nuclear emission. However, bridging the gap between H II region galaxies and AGN are the transition region galaxies; these sources are much more likely to have unresolved nuclei, and possibly represent the "switching on" of AGN in very dense nuclei that are dominated by star formation.

Possibly the greatest question mark surrounding the nature of LLAGN concerns LINERs. Whereas there is little doubt that LINER nuclei that exhibit broad emission lines are powered by AGN (Younes et al. 2011), the origin of the emission in narrow-line LINERs (type 2) is more open to debate. González-Martín et al. (2009b) found that 80 % of their sample of LINERs were AGN, but many alternative theories have been proposed to explain the emission from these objects, such as poststarbursts (Taniguchi et al. 2000) or old stellar populations (Cid Fernandes et al. 2009). González-Martín et al. (2009a) also noted that LINERs may be more heavily obscured than Seyferts. The presence of hard X-ray emission in the nucleus of a LINER is a strong indication of AGN activity, but it does not necessarily follow that the AGN emission is responsible for ionising the narrow line region (NLR). In general, type-2 LINERs are regarded as something of a “mixed bag” and certainly cannot be understood without due consideration of the wider nuclear environments in which they are found.

2.3 The Sample

My sample is based upon the well studied Palomar sample of local galaxies, which was the subject of an extensive spectroscopic survey by Ho et al. (1997a). This sample contains 486 northern galaxies ($\delta \geq 0°$), brighter than $B_T = 12.5$ mag and no further in distance than $\sim$100 Mpc, and provides a variety of nuclear spectral types (H II region nuclei, transition region nuclei, LINERs and Seyfert nuclei).

A nearby galaxy sample such as the one I have chosen to use offers a number of advantages when studying AGN activity. Firstly, at distances of less than $\sim$100 Mpc the host galaxies are easily detectable by ground-based surveys such as Palomar or the Sloan Digital Sky Survey (DSS), and, consequently, the sample is complete and does not suffer from the selection effects that plague surveys at larger redshifts. Secondly, nearby galaxies allow us to probe accretion rates that are several orders of magnitude below the Eddington limit and therefore examine accretion on vastly different scales within the same survey. In addition, the angular resolution of *Chandra* allows us to separate emission associated with the SMBH from the many other sources that surround it and therefore reduce the contamination from nearby XRBs and ultra-luminous X-ray sources (ULXs).

In addition to the main sample, I have also included a small number of Palomar Green (PG) quasars (namely PG 0157 + 001, PG 0844 + 349, PG 1004 + 130, PG 1100 + 772, PG 1115 + 407, PG 1211 + 143, PG 1404 + 226, PG 1512 + 370, PG 1543 + 489 and PG 2112 + 059). Although this chapter focuses heavily upon the Palomar sample, which provides an unbiased view of accretion in the local Universe, the quasars can help provide the high accretion rate perspective when included on the same plots. The distances were estimated using redshift data from the NASA/IPAC Extragalactic Database (NED, with the Hubble constant assumed to be $H_0 = 73\,\mathrm{km\,s^{-1}\,Mpc^{-1}}$), and the black hole masses were taken from Inoue et al. (2007).

2.4 The Optical Emission Lines from AGN

The first step towards understanding AGN comes not from X-ray studies but from an appreciation of their optical spectra. Fortunately, much work has already been done in analysing the optical spectra of the Palomar galaxies, and this has been published in a series of papers (Ho et al. 1997a, b, c, 2009). Figure 2.1 shows the optical spectra of a selection of LINER (left) and Seyfert-1 (right) galaxies (with the stellar contribution subtracted), and highlights some of the emission lines that are

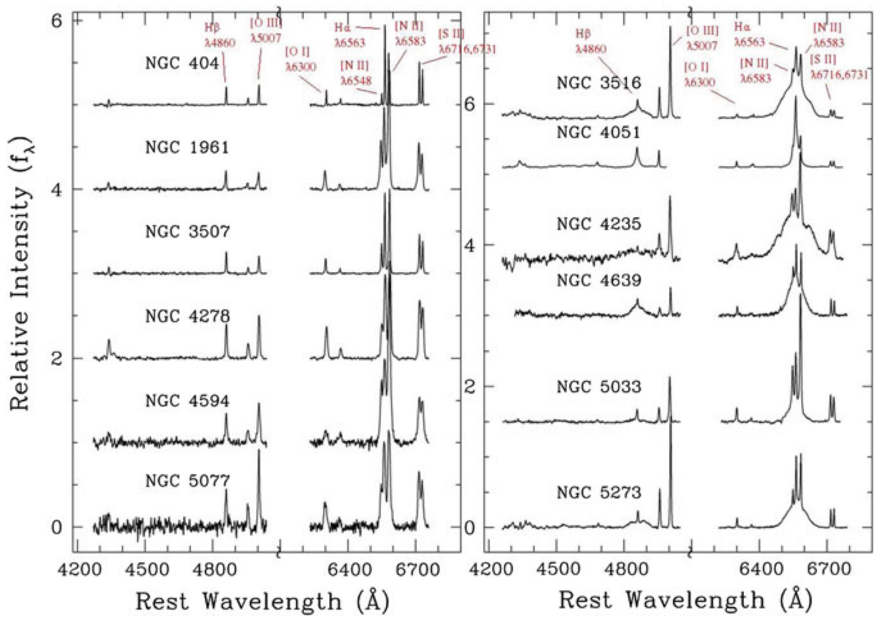

Fig. 2.1 Optical AGN spectra from Ho et al. (1997a) for a selection of LINERs (*left*) and Seyfert-1s (*right*), offset from each other for clarity. The authors have subtracted the stellar contribution from each source by using various nearby absorption line galaxies as templates. The higher ionisation of Seyferts compared to LINERs is clear from the relative strengths of the [O III] and [O I] lines. Both classes can show broad Hα and Hβ lines, but these tend to be stronger in the Seyferts. © AAS. Reproduced with permission

most relevant to this chapter. It can clearly be seen from the relative strengths of the [O III] and [O I] lines that LINERs exhibit lower ionisation that Seyferts, but it is also clear that LINERs can show weak broad Hα lines. The presence of broad lines is probably the most reliable indicator that the emission is from the vicinity of a SMBH, and in Seyfert galaxies the broadening can be as much as FWHM $\approx$ 7,600 km s^{-1} (Ho et al. 1997c).

2.5 Classifying Low Luminosity AGN

Many galaxies in the nearby Universe show emission lines from their nuclei (Ho et al. 1997a detected emission lines in 421 of their 486 sample galaxies), and accretion onto a SMBH is not the only possible explanation for this phenomenon. For instance, the ionisation could be the result of nuclear starbursts, in which a large number of stars are born in a compact area in a short period of time, and subsequently ionise the surrounding gas with powerful winds. Alternatively, it could be the result of a

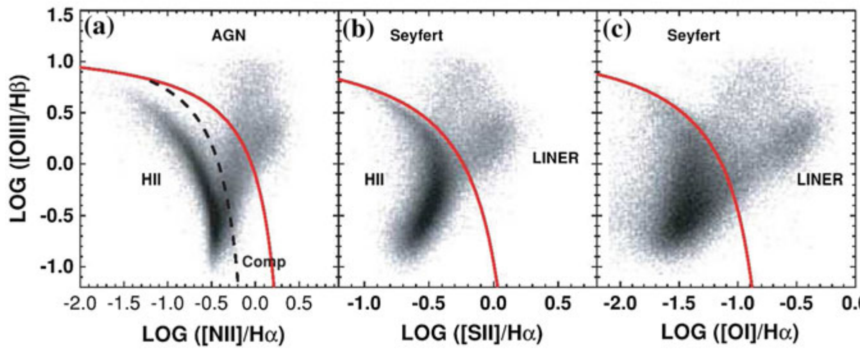

Fig. 2.2 The relative strengths of the emissions lines used as a diagnostic between ionisation due to star formation and accretion (Kewley et al. 2006). Reproduced with permission of Oxford University Press on behalf of the Royal Astronomical Society

high density of XRBs or supernova remnants in the region surrounding the galactic nuclei.

To help make sense of the variety of different properties observed amongst LLAGN, these sources are usually classified using a plot similar to those proposed by Baldwin et al. (1981). This kind of diagnostic diagram has become known as a BPT diagram, and these plots utilise various different emission lines in order to differentiate between ionisation due to star formation and accretion. Typical diagnostics include [N II]/Hα, [S II]/Hα or [O I]/Hα versus [O III]/$H\beta$, as shown in Fig. 2.2 (Kewley et al. 2006).

The Palomar data used within this chapter have already been classified into their various spectral types, and these are supplied in the same paper as the emission line strengths (Ho et al. 1997a). However, these classifications are based upon line strength ratios that have not been corrected for reddening (see Richings et al. 2011) and, therefore, I instead choose to use classifications that are based upon the extinction-corrected data. These data have been provided by Phil Uttley (private communication), along with the de-reddened emission line strengths. The latter were corrected for extinction using the extinction law of Cardelli et al. (1989), and spectral classifications assigned to each source using the BPT diagnostic diagrams of Kewley et al. (2006). Figure 2.3 shows the [N II]/Hα versus [O III]/Hβ diagnostic for the complete Palomar sample.

Using this new classification scheme based upon extinction-correction line ratios I find that I have 142 H II region nuclei, 73 transition region nuclei, 134 LINERs, 56 Seyfert nuclei and 81 unknowns. The ‘unknowns’ include the 79 galaxies from which Ho et al. (1997a) detected no visible emission lines (or only very weak emission lines).

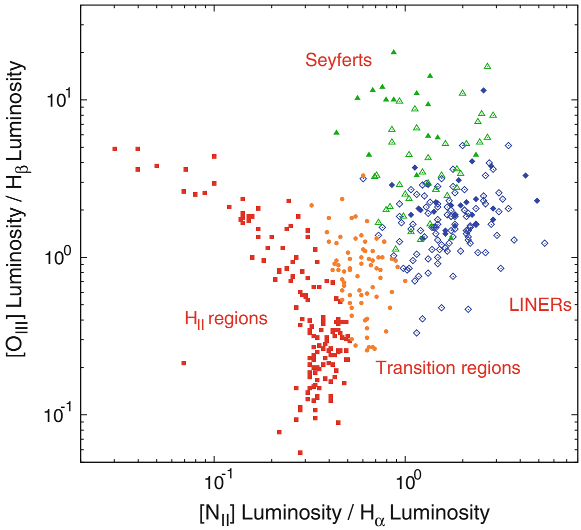

Fig. 2.3 Re-classified, extinction corrected BPT diagram for the complete Palomar sample. *Red squares* are H II regions, *orange circles* are transition regions, *blue diamonds* are LINERs (*filled* are type 1, *unfilled* type 2) and *green triangles* are Seyferts (*filled* are type 1, *unfilled* type 2). The H II regions sweep from the *top left* to the *bottom* of the plot (referred to as the star-forming sequence by Kewley et al. (2006)) and the Seyferts and LINERs occupy the *upper-right* region of the plot

2.6 The Optical Lines as Indicators of X-ray Luminosity

The X-ray luminosity from AGN, and especially at energies above 2 keV, is often used as a reliable indicator of accretion rate. The reason that this region of the electromagnetic spectrum is particularly suitable for this purpose is due to the origin of the X-ray emission, which is believed to be produced on scales comparable to the accretion flow through processes such as inverse Compton scattering of lower energy seed photons in a corona of hot electrons or blackbody emission from the accretion disc. Furthermore, the energetic nature of X-ray photons enables them to penetrate the often dense clouds of gas and dust that may surround a SMBH and therefore provide a direct view of the innermost regions of the system.

In some sources, however, the column density ($N_{\rm H}$) is so high (presumably the result of matter predominantly in the vicinity of the SMBH) that not even X-ray photons in the typical 0.3–10 keV sensitivity range of a modern X-ray telescope such as *Chandra* are able to penetrate. In this scenario, which occurs when $N_{\rm H}$ exceeds $\sim 10^{24}\,\rm cm^{-2}$, the source is said to be Compton thick and the intrinsic X-ray flux below 10 keV is completely absorbed, replaced instead by a combination of scattered and reflected emission which is expected to be a couple of orders of magnitude weaker than the intrinsic emission. However, under the standard model of AGN (Antonucci and Miller 1985) the absorbing matter takes the form of a torus, and therefore a column density $\geq 10^{24}\,\rm cm^{-2}$ in the observer's line of sight will not

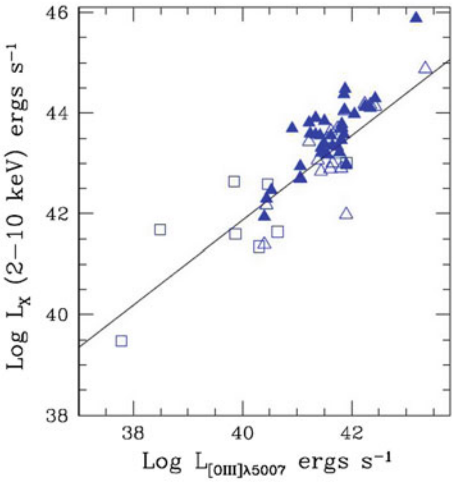

Fig. 2.4 Plot of $L_{[\mathrm{O\,III}]}$ versus L_{X} for three samples of Seyfert-1 (Georgantopoulos and Akylas 2010). Reproduced with permission © ESO

prevent the ionisation of the NLR which surrounds the whole system to a distance of up to $\sim$100 pc.

The strengths of various optical emission lines originating in the NLR, in particular the Balmer lines (H α and H β) and [O III]$_{\lambda 5007}$, have often been used as good isotropic indicators of X-ray luminosity or AGN power (e.g. Panessa et al. 2006; González-Martín et al. 2009b). The strength of the correlation between the 2–10 keV X-ray luminosity and the optical lines is particularly strong amongst sources that also exhibit broad emission lines in their optical spectra, the presence of which is probably the clearest indication one can get that an AGN is responsible for the X-ray emission. Figure 2.4 shows the correlation between $L_{2-10\,\mathrm{keV}}$ and $L_{[\mathrm{O\,III}]\lambda 5007}$ for three samples of Seyfert-1, demonstrating the tight correlation that is often found between these properties in unobscured sources. Many authors have also examined the correlation between X-ray luminosity and H α luminosity (e.g. Ho et al. 2001; Panessa et al. 2006; Terashima et al. 2000) and found that it persists down to bolometric luminosities as low as 10^{37} erg s^{-1}.

A reliable indicator of intrinsic X-ray luminosity is a valuable tool in identifying Compton-thick AGN. The standard model predicts that the NLRs of sources that are heavily obscured ($N_{\mathrm{H}} \geq 10^{24}\,\mathrm{cm}^{-2}$) by the torus will still be ionised by the X-ray emission from the central engine along the less obscured axis perpendicular to the observer's line of sight. These Compton-thick sources will be expected to show $L_{[\mathrm{O\,III}]}/L_{\mathrm{X}}$ ratios that are significantly greater than for those where lower obscuration allows the intrinsic X-ray emission to be viewed directly.

2.7 Data Reduction

2.7.1 Observation Selection

In order to ensure a consistent approach throughout it was decided to use only observations made with the Advanced CCD Imaging Spectrometer (ACIS) instrument and neglect those that used the High Resolution Camera (HRC), which, in any case, has rarely been used to observe any of the sources in my sample. The *Chandra* archive was searched for each of the sources and suitable observations were identified and retrieved. In general, observations with particularly short exposure times ($<\sim 2$ ks) were ignored, but, in anticipation of the effect of pileup on the brighter sources, observations with short frame times or those which utilised the High Energy Transmission Grating (HETG) were also desirable.

2.7.2 Image Analysis

For each observation the level 2 event data were examined in DS9 and source and background regions were placed around the X-ray point source that was thought to represent emission from the central engine. In all cases I took the presence of an unresolved nuclear source in the 2–10 keV band as evidence of AGN activity, and, although identification of the nucleus was generally straightforward, for some sources it was necessary to reference the literature for a more precise location. In most cases a circle of radius $1.5''$ was used to describe the source region and an annulus of between 8 and $12''$ was used for the background region, but this varied slightly depending upon the proximity of nearby sources. Observations in which no unresolved emission was detected were ignored, as were those of NGC 4151 and NGC 4486 due to the severe effects of pileup. An unresolved X-ray nucleus could be identified with confidence in 89 sources.

Data reduction was performed using CXC *Chandra* Interactive Analysis of Observations (CIAO) software version 4.2. After restricting the event files to the energy range 0.3–10 keV the script PSEXTRACT was then used to automatically generate grouped spectra with 15 counts per channel. In most cases it was necessary to recreate the response matrix file (RMF) and ancillary response function (ARF) files manually using the CIAO tools MKACISRMF and MKARF respectively.

2.7.3 Spectral Fitting

Once spectra had been extracted the fitting was performed using XSPEC version 12.6.0 over the energy range 0.3–10 keV. Each source was initially fitted with a model comprising Galactic absorption (PHABS) fixed to column densities obtained using the NH program from the NASA HEASARC FTOOLS software[1] (Blackburn 1995), a power law component (ZPOWERLW) and a second absorption component (ZPHABS) representing absorption in the host galaxy. In some cases additional components were included such as an iron K α line at 6.4 keV (modelled with ZGAUSS) or a thermal component (MEKAL) but these were only used if the spectrum had sufficient counts to justify the extra parameters and the quality of the fit was significantly improved.

For each observation the ratio of the bolometric luminosity to the Eddington luminosity serves as a proxy for accretion rate (see Chap. 1 for a discussion of how luminosity relates to $\dot{m}_{\rm E}$), and is estimated using

$$\frac{L_{\rm bol}}{L_{\rm Edd}} = \frac{F_{2-10\ {\rm keV}} \times 4\pi d^2}{L_{\rm Edd}} \times C_{2-10\ {\rm keV}} \tag{2.1}$$

where $F_{2-10\,{\rm keV}}$ is the 2–10 keV flux from the *Chandra* fit, d is the distance to the galaxy (from Ho et al. 1997a), $C_{2-10\,{\rm keV}}$ is the bolometric correction (see below) and $L_{\rm Edd}$ is the Eddington limit for the source given by

$$L_{\rm Edd} = \frac{4\pi\, G M_{\rm BH}\, m_{\rm p}\, c}{\sigma_{\rm T}} \tag{2.2}$$

where G is the gravitational constant, $M_{\rm BH}$ is the black hole mass, $m_{\rm p}$ is the mass of a proton and $\sigma_{\rm T}$ is the Thompson scattering cross-section for an electron. For each source, $M_{\rm BH}$ was estimated using the relation between black hole mass and velocity dispersion (σ, obtained for the Palomar sample from Ho et al. (2009)) given by Tremaine et al. (2002), namely

$$\log \frac{M_{\rm BH}}{M_\odot} = \alpha + \beta \log \frac{\sigma}{\sigma_0} \tag{2.3}$$

where $\alpha = 8.13 \pm 0.06$, $\beta = 4.02 \pm 0.32$ and $\sigma_0 = 200\,{\rm km\,s^{-1}}$. The bolometric correction, $C_{2-10\,{\rm keV}}$, is estimated using the relation from Marconi et al. (2004), rearranged to

$$\log C_{2-10\,{\rm keV}} = \log \frac{L_{\rm bol}}{L_{2-10\,{\rm keV}}}$$
$$\log C_{2-10\,{\rm keV}} = 2.98 - 0.264 \log L_{\rm bol} + 0.03 \log^2 L_{\rm bol} - 0.0015 \log^3 L_{\rm bol} \tag{2.4}$$

where $L_{\rm bol}$ is the bolometric luminosity in units of $L_\odot$. Equation 2.4 must be solved iteratively in order to find $L_{\rm bol}$ from the known $L_{2-10\,{\rm keV}}$.

[1] http://heasarc.gsfc.nasa.gov/ftools/.

2.8 Distribution of M_{BH}, Eddington Ratio and N_{H} for the Palomar Sample

Amongst the properties derived directly from the spectral fits to the *Chandra* data are the source flux ($F_{2-10\,\mathrm{keV}}$), the photon index (Γ), the iron K α line width and the absorbing column density (N_{H}). To these results I add data from the literature, such as the colour excess ($E(B-V)$), host galaxy morphology, emission line luminosity (H α, H β, $[\mathrm{O\,III}]_{\lambda 5007}$, $[\mathrm{N\,II}]_{\lambda 6583}$ and the sum of $[\mathrm{S\,II}]_{\lambda 6716}$ and $[\mathrm{S\,II}]_{\lambda 6731}$), source distance (all Ho et al. 1997a), velocity dispersion (σ) (Ho et al. 2009) and 15 GHz radio luminosity (Nagar et al. 2005). From these data I then derive the luminosity ($L_{2-10\,\mathrm{keV}}$), the black hole mass (M_{BH}) and the Eddington ratio ($\lambda = L_{\mathrm{bol}}/L_{\mathrm{Edd}}$).

Figure 2.5 (left) shows a histogram of M_{BH} for the complete Palomar sample, broken down by spectral classification. The range of masses over which each spectral type is distributed can be explained by the possible evolutionary sequence from H II regions to transition regions, to Seyfert galaxies, and finally to LINERs (e.g. Constantin et al. 2009). In particular, there is very little overlap in M_{BH} between the LINERs and H II regions, both of which occupy the low accretion rate end of the scale ($\lambda \leq 10^{-3}$).

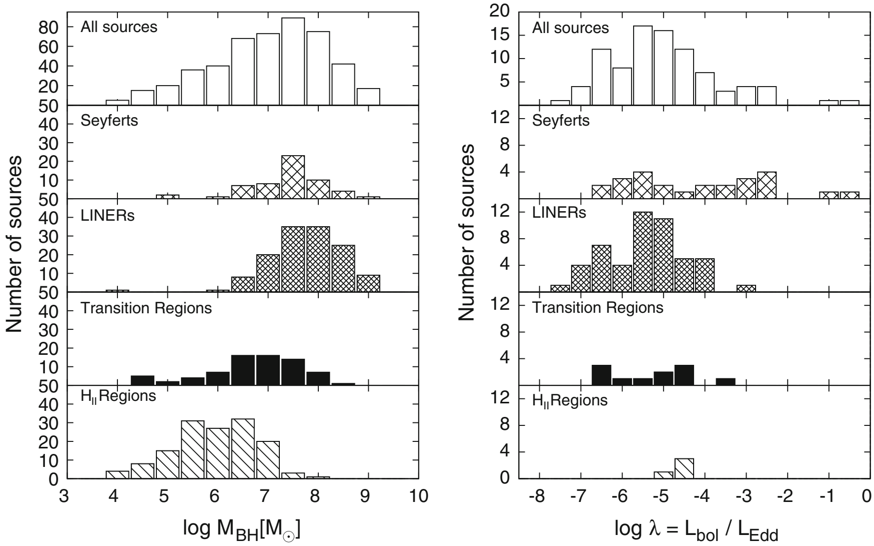

Fig. 2.5 *Left* Histogram of black hole mass for the complete sample. LINERs and H II regions generally do not overlap much in black hole mass, with the latter occupying the high-mass end of the scale. *Right* Histogram of Eddington ratio from the *Chandra* analysis of the sample. The Seyferts extend over a much larger range of λ than the other spectral types, and appear to show a slightly bimodal distribution (the distribution can be fitted with two Gaussian components, centred on $\log \lambda = -2.95$ and -5.65; I find that an F-test rejects a single-Gaussian fit at the 1-σ level); both of these facts can be attributed to absorption, with the unobscured Seyfert-1s mostly occupying the $\lambda \geq 10^{-4}$ end of the scale and the Seyfert-2s the $\lambda \leq 10^{-4}$ end

Figure 2.5 (right) shows a histogram of Eddington ratio ($\lambda = L_{bol}/L_{Edd}$) from the *Chandra* analysis of the sample. Whereas the transition regions, LINERs and H II regions are generally low Eddington ratio ($\lambda \leq 10^{-3}$), the Seyfert galaxies cover a much wider range spanning several orders of magnitude. The Seyfert galaxies also show a bi-modal distribution in λ, with the type-1 Seyferts found at high Eddington ratios ($\lambda \geq 10^{-4}$) and the type-2 Seyferts found at low Eddington ratios ($\lambda \leq 10^{-4}$).

The slight differences in M_{BH} and λ between different spectral types are more clearly seen when the two parameters are plotted against each other (Fig. 2.6). In this plot I have marked regions where the different spectral types are generally found, and there appears to be a fairly clear distinction between the quasars, type-1 Seyferts, H II regions and LINERs, with the transition regions and type-2 Seyferts more scattered.

The standard model of AGN asserts that many of the differences in fundamental properties that we observe in these sources can be explained as an effect of inclination, and the lack of broad optical emission lines in type-2 sources is simply a result of obscuration by the torus. If this is true, it would therefore be reasonable to expect that type-2 sources should, on average, exhibit greater absorption than type-1

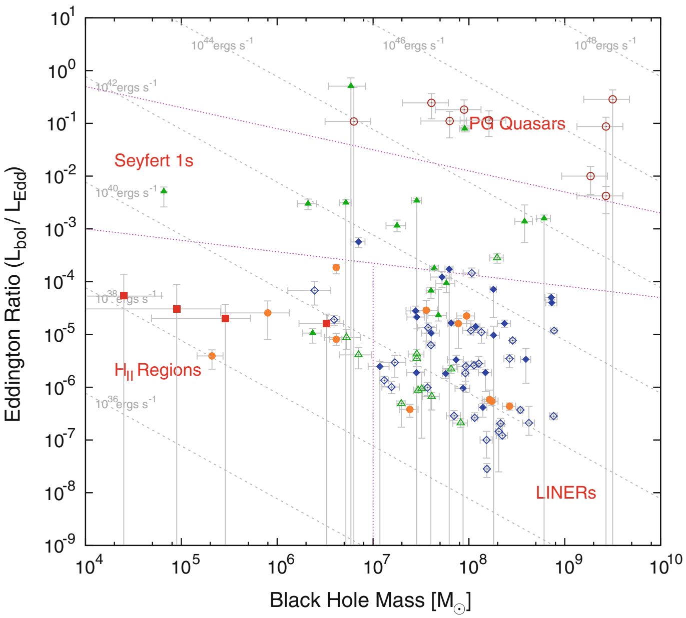

Fig. 2.6 Plot of black hole mass M_{BH} versus Eddington ratio $\lambda = L_{bol}/L_{Edd}$ (serving as a proxy for accretion rate) for the Palomar sample galaxies and a small selection of PG quasars. The quasars (*open red circles*), Seyfert-1s (*filled green triangles*), LINERs (*filled* and *open blue circles*, representing type 1 and type 2 respectively) and H II region nuclei (*red squares*) are generally found in different regions of the plot. The remaining symbols represent Seyfert-2s (*open green triangles*) and transition region nuclei (*orange circles*)

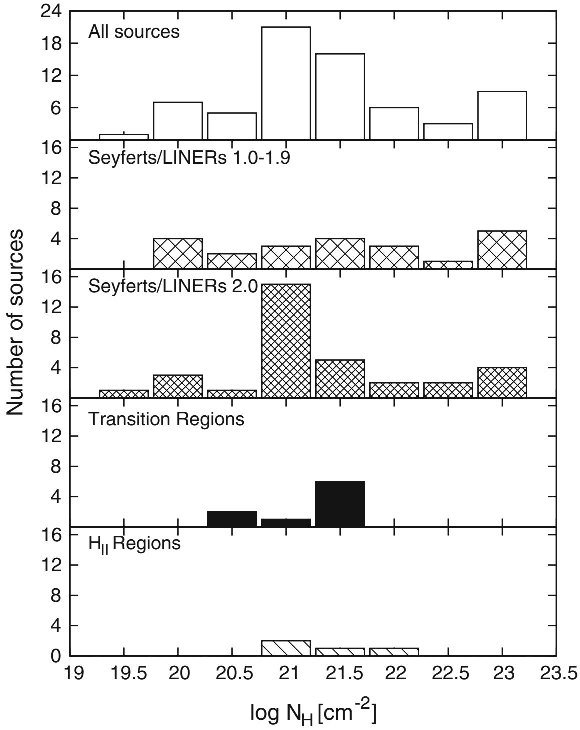

Fig. 2.7 Histogram of X-ray column density (N_H) for the complete sample, and also broken down by spectral type. Seven sources were excluded because the fits to the soft emission were too uncertain to obtain a reliable estimate of the absorption, and a further ten sources (7 type-1, 2 type-2 and 1 transition region) appeared to show no absorption

sources. However, there is always a degree of uncertainty over any measurement of the column density, especially when $N_H \leq \sim 10^{23}$ cm^{-2}; to fit an absorption model one must know the exact form of the underlying continuum, a challenge that is made more difficult by the presence of soft emission of a fairly uncertain nature in many AGN.

Figure 2.7 shows a histogram of the absorbing column density (N_H), measured directly from the *Chandra* spectral fits. The type-2 AGN, transition regions and H II regions generally show a quite narrow range of absorption, with 30 of the 46 sources (65 %) from which the absorption could be measured having a column density of between $10^{20.75}$ and $10^{21.75}$ cm^{-2}. This level of absorption is within an order of magnitude of Galactic absorption, and is therefore not unexpected in the region of a galaxy nucleus; a column density of $\sim 10^{21}$ cm^{-2} could easily be produced by dust lanes, for instance.

In contrast, the type-1 sources exhibit a much greater variety of column densities and show no evidence of being less absorbed than their type-2 counterparts.

Figure 2.7, however, does not show the intrinsic absorption of sources that are Compton thick; these sources may instead appear on the plot with much lower column densities, representing the absorption that affects the reprocessed emission as X-rays are scattered or reflected into our line of sight. Furthermore, there are ten sources (7 type-1, 2 type-2 and 1 transition region) where the absorption is too low to be detectable (usually due to having too few photons to avoid heavy rebinning of the data), and these have been excluded from the plot.

2.9 Identifying the Compton-Thick AGN in Our Sample

It is unfortunate that, in order to assess the effectiveness of a particular technique for identifying Compton-thick AGN, one must first apply another—possibly equally uncertain—technique in order to determine which members of the sample are indeed Compton thick. A good indicator of heavy absorption is the presence of polarised broad lines in the optical spectrum (Antonucci and Miller 1985), and when combined with an X-ray column density that appears very low then Compton thickness is almost assured. However, the detection of polarised broad lines is only possible in the brightest sources and there is currently very little spectropolarimetric data in the literature for sources within my sample.

Another useful indicator of Compton thickness is the presence of hard X-ray emission ($>$10 keV) from a source which is relatively weak at softer energies; this hard emission can penetrate an absorbing column that is dense enough to block the 2–10 keV emission that is within the peak sensitivity range of observatories such as *Chandra* and *XMM Newton*. Surveys such as the *Swift* BAT survey (Baumgartner et al. 2012) have produced catalogues of X-ray sources at energies above 14 keV, and 17 of the 89 sources for which I have obtained Chandra spectra are found amongst the 1,171 sources detected by BAT. Figure 2.8 shows a plot of the 2–10 keV *Chandra* luminosity from my survey against the 14–195 keV *Swift* BAT luminosity (Baumgartner et al. 2012).

Ultimately, AGN are classified as Compton thick or Compton thin depending upon evidence from multiple indicators and, initially, I choose to select the Compton-thick sources in my sample using the 0.3–10 keV spectra. Figure A.1 in Appendix A shows the *Chandra* spectra of 11 sources that have at least one of two Compton-thick indicators, which are a flat spectrum above 2 keV and a large iron K α line equivalent width. Five of these sources (NGC 1052, NGC 1068, NGC 3079, NGC 4102 and NGC 7479) were also detected by the BAT survey with larger than average ratios of $L_{14-195\,\rm keV}/L_{2-10\,\rm keV}$ (Fig. 2.8).

After Compton-thick candidates had been identified from their *Chandra* spectra, I next performed a literature search in order to verify or reject those sources. Aside from the archetypal Compton-thick Seyfert-2, NGC 1068 (for which this step wasn't considered necessary), this provided support for the inclusion of NGC 2782 (Zhang et al. 2006), NGC 3079 (Iyomoto et al. 2001), NGC 3690 (Della Ceca et al. 2008), NGC 4036 (González-Martín et al. 2009a), NGC 4102 (González-Martín et al. 2011),

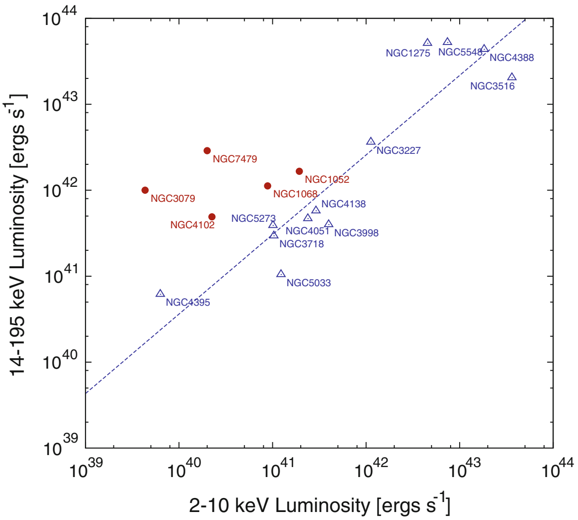

Fig. 2.8 Plot of the 2–10 keV *Chandra* luminosities from my survey against the 14–195 keV *Swift* BAT luminosities from Baumgartner et al. 2012. Sources with *Chandra* spectra that show signs of Compton thickness, such as a flat spectrum above 2 keV or a large iron K α line equivalent width, are plotted with *filled red circles* and sources that show no such signs are plotted with *open blue triangles*. A linear fit to the latter has equation $\log L_{14-195\,\mathrm{keV}} = 3.54 + 0.93 \log L_{2-10\,\mathrm{keV}}$

NGC 4501 (Brightman and Nandra 2008), NGC 5194 (Cappi 2006) and NGC 7479 (Georgantopoulos et al. 2011). However, the classification of two further sources, NGC 1052 and NGC 4111, is more uncertain. González-Martín et al. (2009a) found that, for both these sources, the only indication of Compton thickness is their unusually flat spectra, and other common indicators suggest that they are in fact Compton thin. In this chapter I include both these sources in my list of likely Compton-thick candidates, but highlight instances where their properties are inconsistent with the other 9 sources.

2.10 The Relationship between $L_{2-10\,\mathrm{keV}}$ and $L_{[\mathrm{O\,III}]}$ and its use as an Absorption Indicator

The emission line most commonly used as an indicator of intrinsic X-ray luminosity is the [O III] forbidden line of doubly ionised oxygen (e.g. see Bassani et al. 1999; Georgantopoulos and Akylas 2010; González-Martín et al. 2009b; Panessa and Bassani 2002; Panessa et al. 2006), emitted in the green part of the optical spectrum at 500.7 and 495.9 nm. In this thesis I use only the 500.7 nm line intensities, which were published for the entire Palomar sample by Ho et al. (1997a).

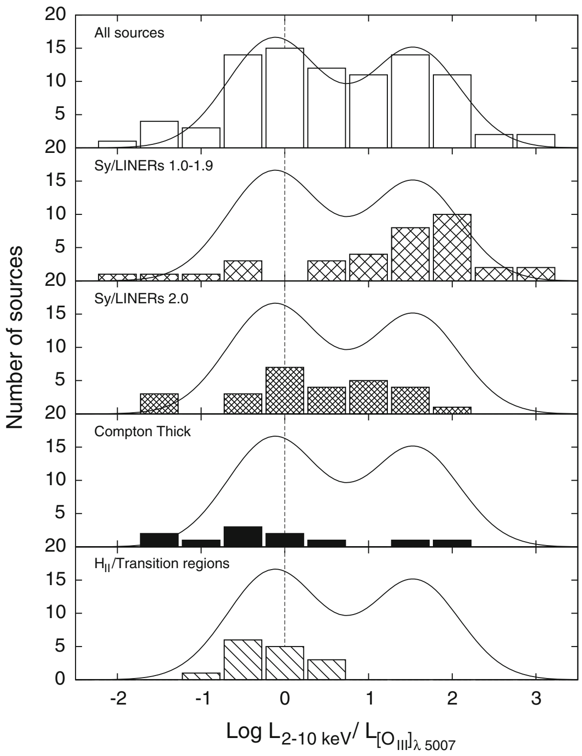

Fig. 2.9 Histogram showing the ratio of X-ray luminosity to [O III]$_{\lambda 5007}$ luminosity. *Top panel* All sources for which *Chandra* spectra were extracted. The distribution appears slightly bimodal and has been fitted with two Gaussians (centred at −0.129 and 1.549), which are shown in each of the panels (*black line*). *Second panel* Sources classified as either Seyfert 1.0–1.9 or LINER 1.0–1.9. I find a mean $\log_{10} L_{2-10\,\mathrm{keV}}/L_{[\mathrm{O\,III}]}$ ratio of 1.23. *Third panel* Sources classified as either Seyfert-2 or LINER-2. I find a mean $\log_{10} L_{2-10\,\mathrm{keV}}/L_{[\mathrm{O\,III}]}$ ratio of 0.344. *Fourth panel* Sources with X-ray spectra showing evidence of Compton thickness, such as a flat spectrum above 2 keV or a large iron K α line equivalent width. I find a mean $\log_{10} L_{2-10\,\mathrm{keV}}/L_{[\mathrm{O\,III}]}$ ratio of −0.178. *Bottom panel* Sources classified as either H II region or transition region nuclei, in which emission associated with stellar processes would be expected to contribute greatly to the optical emission line strength. I find a mean $\log_{10} L_{2-10\,\mathrm{keV}}/L_{[\mathrm{O\,III}]}$ ratio of −0.199. Compton-thin sources that are powered by an AGN tend to have X-ray/[O III] ratios that are scattered about the second Gaussian peak, whereas sources that are believed to be Compton thick are more scattered. However, the spectral classifications most strongly clustered about the first Gaussian peak are the H II/transition region nuclei, raising the possibility that star formation may be a significant factor in producing the double-Gaussian distribution of the $L_{2-10\,\mathrm{keV}}/L_{[\mathrm{O\,III}]}$ histogram in LLAGN

Previous studies of the relationship between $L_{2-10\,\mathrm{keV}}$ and $L_{[\mathrm{O\,III}]}$ have reported upon a bimodal distribution in the histogram of $R_{\mathrm{X}/[\mathrm{O\,III}]} = L_{2-10\,\mathrm{keV}}/L_{[\mathrm{O\,III}]}$ (e.g. Maiolino et al. 1998; González-Martín et al. 2009b), which the authors associate with the presence of Compton-thick and Compton-thin populations in the sample. In Fig. 2.9 I find only a slight suggestion of bimodality in my data, and fit the histogram of all sources with two Gaussian components (centred at $\log R_{X/[O\,III]} = -0.129$ and 1.549). However, an F-test fails to reject a single-Gaussian fit at the 1–σ level.

When the data are broken down by spectral classification it can be seen that the sources for which we can say with greatest certainty that the X-ray emission originates from an accretion flow (Seyferts and LINERs, types 1.0–1.9) show the highest $L_{2-10\,keV}$ to $L_{[O\,III]}$ ratios ($\overline{\log R_{X/[O\,III]}} = 1.23$), and are clustered around the second Gaussian peak. The lowest ratios are found in the H II regions/transition regions and the Compton-thick sources ($\overline{\log R_{X/[O\,III]}} = -0.199$ and -0.178 respectively) and the former are strongly clustered about the first Gaussian peak (more so than the Compton-thick sources, which are more spread out). These results suggest that star formation (which is expected to contribute strongly to the [O III] emission of H II region and transition region nuclei) may be responsible for the double-Gaussian distribution of the $L_{2-10\,keV}/L_{[O\,III]}$ histogram in LLAGN, bringing into question the validity of using this ratio as a Compton-thick diagnostic.

In Fig. 2.10 I plot $L_{2-10\,keV}$ against $L_{[O\,III]\lambda5007}$, dividing the sources into type-1 and 2 AGN, starburst sources (H II regions and transition regions) and Compton-thick AGN. The solid red line corresponds to the local minimum between the two

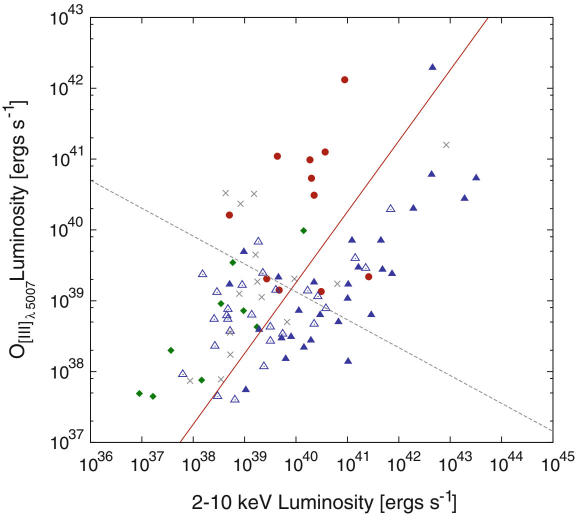

Fig. 2.10 2–10 keV X-ray luminosities from my *Chandra* survey plotted against the luminosity of the $[O\,III]_{\lambda5007}$ emission line (from Ho et al. 1997a). The *red line* ($L_{[O\,III]} = 0.181\,L_{2-10\,keV}$) corresponds to the minimum in the double-Gaussian fit to the $L_{2-10\,keV}/L_{[O\,III]}$ histogram. Type-1.0–1.9 LINERs and Seyferts are shown with *filled blue triangle*, type-2 LINERs and Seyferts with *open blue triangles* and H II/transition region nuclei with *filled green diamonds*. The sources selected as Compton-thick candidates are marked with *filled red circles*. Any observations with fewer than 100 counts, in which the spectra were not of sufficient quality to identify Compton-thick candidates, are marked with *grey crosses*. Most of the Compton-thick sources are found in the region $L_{[O\,III]} \geq 0.181\,L_{2-10\,keV}$, but are clearly distinct in their [O III] luminosity from Compton-thin sources (shown separated by the *dashed grey line*), suggesting that the usefulness of the X-ray/[O III] ratio as a Compton-thick diagnostic may not extend down to LLAGN

Gaussian components that were fitted to the $L_{2-10\,\mathrm{keV}}/L_{[\mathrm{O\,III}]}$ histogram (Fig. 2.9), and most of the Compton-thick candidates lie to the left-hand-side of this line. However, amongst the sources on the left-hand-side of the red line (sources where $L_{[\mathrm{O\,III}]} \geq 0.181\, L_{2-10\,\mathrm{keV}}$), there is a clear distinction in luminosity between Compton-thick and Compton-thin sources, with the former being found at higher luminosities. This division in luminosity between Compton-thick and Compton-thin sources (shown with a dashed grey line) also marks a change in the distribution of sources for the sample as a whole. At higher luminosities there is a noticeable gap in the density of points with mostly type-1 AGN to the right-hand-side of the red line and mostly Compton-thick AGN to the left-hand-side. A histogram of $L_{\mathrm{X}}/L_{[\mathrm{O\,III}]\lambda 5007}$ for these data would produce a far clearer bimodal distribution than the one I find in Fig. 2.9. However, at lower luminosities (beneath the dashed grey line) this gap disappears and the data points become more evenly spread. Here I find an absence of Compton-thick sources, replaced instead by a population of starburst sources (H II/transition region nuclei), all of which are found to the left-hand-side of the red line. This result is consistent with recent studies (e.g. Hopkins et al. 2009; Panessa and Bassani 2002) which report that LLAGN that are heavily obscured by the torus are less common than previously thought.

The picture that emerges from these data is that the $L_{2-10\,\mathrm{keV}}/L_{[\mathrm{O\,III}]}$ ratio diagnostic of Compton thickness is only valid above $L_{[\mathrm{O\,III}]} \approx 10^{39}\,\mathrm{erg\,s^{-1}}$. At lower luminosities, starburst contamination creates considerably more scatter in the data and the likely disappearance of the torus means that we no longer see a separate population of sources representing the Compton-thick candidates. In this luminosity regime, the standard model of Antonucci and Miller (1985) no longer applies and the $L_{2-10\,\mathrm{keV}}/L_{[\mathrm{O\,III}]}$ ratio may instead be useful in separating starburst nuclei from AGN.

The similarity of the X-ray to [O III] ratios in Compton-thick sources and starburst sources (H II regions/transition regions) may suggest a connection between the two, further evidence for which is provided by the breakdown of Compton-thick sources by spectral type, which reveals that 33 % (3 from 9) of transition regions for which I have spectra available and at least 100 spectral counts are actually Compton thick. This figure is comparable to that found for Seyferts of type 1.8–2.0, where 23 % (3 from 13) appear Compton thick, and higher than for the other spectral types, with 0 % (0 from 7) of Seyferts of type 1.0–1.5 and 10 % (4 from 41) of LINERs also appearing Compton thick. Only three H II regions have at least 100 spectral counts, and none of these appear Compton thick.

2.11 A Comparison of Absorption in the X-ray and Optical Bands

The X-ray emission from an accreting black hole is believed to arise in the innermost regions of the accretion flow ($\leq$1 pc) where the in-falling material is at its hottest. In contrast, the narrow emission lines (such as H α, H β, [O III], [N II], [S II], etc.) observed from AGN are produced in the NLR at distances of up to $\sim$100 pc from the black hole. Therefore, it should be expected that, even in sources where the alignment of the torus is such that it does not obscure the emission from the central engine, the X-ray emitting region should be more heavily obscured than the NLR.

Absorption in the X-ray band is mostly due to the presence of gas between the source and the observer, which is quantified in terms of its hydrogen column density ($N_{\rm H}$) in units of atoms per cm^2. Extinction in the optical band is mostly due to dust and is estimated from the colour excess

$$E(B-V) = (B-V)_{\rm observed} - (B-V)_{\rm intrinsic} \tag{2.5}$$

where $B-V$ is the difference between the magnitudes in the B and V filters. The gas and dust that are responsible for X-ray and optical extinction respectively usually exist together in a ratio that is reasonably consistent (at least, the estimates of this ratio from the literature vary by a factor of less than ~5, which is small when compared to the scatter found in my data). In this chapter I choose to use the empirical relationship of Bohlin et al. (1978) ($N_{\rm H}/E(B-V) = 5.8 \times 10^{21}$ cm^{-2} mag^{-1}), but I could also have chosen Predehl and Schmitt (1995) ($N_{\rm H}/E(B-V) = 1.79 \times 10^{21}$ cm^{-2} mag^{-1}).

Figure 2.11 shows a histogram of the ratio between $N_{\rm H}$ and $E(B-V)$, broken down to separately show Compton-thin sources with low and high X-ray to [O III] ratios (where $L_{\rm [O\,III]} = 0.181\, L_{2-10\,\rm keV}$ is the boundary between the two). Also shown on the same plot is the Bohlin et al. (1978) relationship between $N_{\rm H}$ and $E(B-V)$ (dotted red line). The Seyferts and LINERs with high X-ray to [O III] ratios (i.e. the sources clustered under the second Gaussian peak of Fig. 2.9) have much higher $N_{\rm H}/E(B-V)$ ratios than we would expect if the same material were responsible for both the X-ray and optical extinction. These sources undoubtedly contain a high proportion of AGN, with broad optical lines detected in 23 of 36 sources (64 %) compared to just 5 of 28 (18 %) in the sources with low X-ray to [O III] ratios, and this 'excess' of X-ray absorption is due to the origin of the X-rays being deep within the AGN where the photons are subjected to much greater obscuration than that which affects the narrow line region further out.

2.12 The Unusual Case of the Seyfert-2 Galaxy NGC 3147

Figure 2.11 also reveals that there are four sources (NGC 1068, NGC 2782, NGC 3147 and NGC 3998) which have X-ray column densities that are more than an order of magnitude less than we would expect from their optical extinction. Although the spectral fit for NGC 2782 is somewhat uncertain in the soft X-ray band (see Appendix A), the X-ray absorption affecting the other three sources is very well constrained.

Figure 2.12 (left) shows the X-ray spectrum of NGC 3147 with the absorbing column density of 1.217×10^{20} cm^{-2} obtained from a free fit. On the right-hand-side of the same figure $N_{\rm H}$ has been fixed to 3.074×10^{21} cm^{-2}, which is the value we would expect from applying the relationship of Bohlin et al. (1978) to the colour excess ($E(B-V) = 0.53$). The higher value of $N_{\rm H}$ provides a poor fit to the data

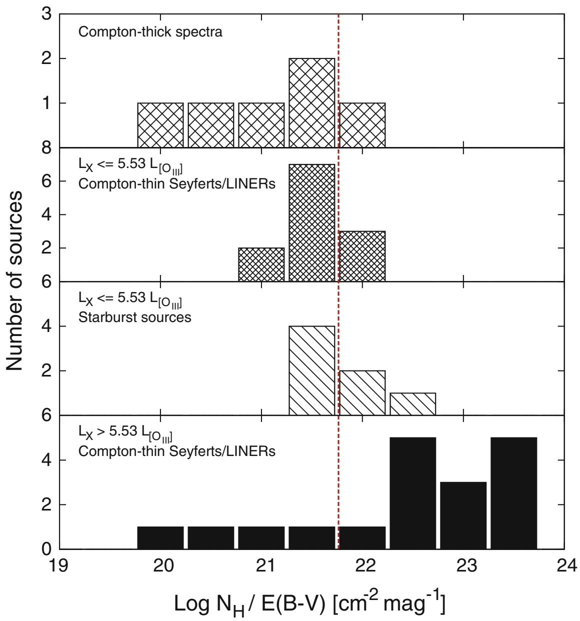

Fig. 2.11 Histogram showing the ratio of column density (N_H) to colour excess ($E(B\text{-}V)$, Ho et al. 1997a). *Top panel* Sources with X-ray spectra that show evidence of Compton thickness. *Second panel* AGN (Seyferts and LINERs) with low X-ray to [OIII] ratios and X-ray spectra that do not show evidence of Compton thickness. The only type-1 Seyfert in this population is NGC 1275, the central member of the Perseus cluster. *Third panel* Starburst sources (H II/transition regions). *Bottom panel* AGN with high X-ray to [O III] ratios, most of which are classified as type-1 Seyferts or LINERs. The *vertical red line* at 5.8×10^{21} cm^{-2} mag^{-1} shows the known empirical relationship between column density and colour excess (Bohlin et al. 1978). Seyferts/LINERs with high X-ray to [O III] ratios generally show much higher absorption in the X-ray band than in the optical, presumably due to the origin of the X-rays being deep within the AGN where the photons are subjected to much greater obscuration than that which affects the *narrow line* region further out. Seyferts/LINERs with low X-ray to [O III] ratios instead show $N_H/E(B-V)$ ratios that are consistent with absorption by the same material in both X-ray and optical bands

at low energies and the source therefore exhibits much lower extinction in the X-ray band than in the optical. Clearly this discrepancy between the X-ray and optical observations of this source cannot be attributed to uncertainty in fitting the X-ray absorption component.

The X-ray emission from AGN is generally believed to come from the innermost regions of the system and, even if the X-ray source in NGC 3147 is unobscured within the inner few parsecs, we would still expect there to be absorption from the same material (perhaps the NLR) that is responsible for the reddening of the Balmer lines. Of course, it is possible that the narrow Balmer lines that are used to estimate $E(B-V)$ may not originate from the vicinity of the central black hole, but the *Chandra* ACIS image shown in Appendix B fails to identify any other strong, compact X-ray sources within a radius of 30 arcseconds of the central source (about 6 kpc at

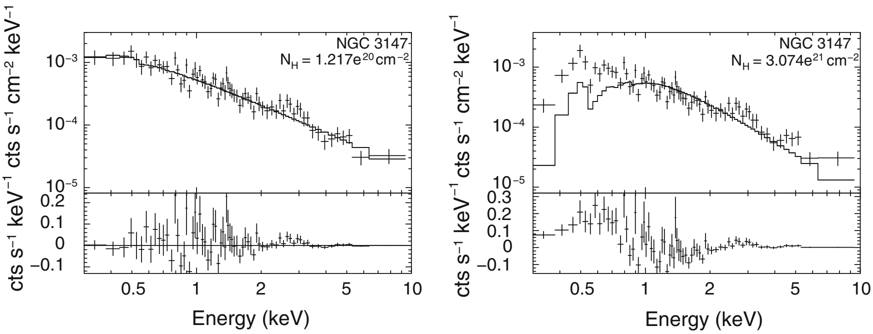

Fig. 2.12 *Chandra* spectrum of the Seyfert-2 galaxy NGC 3147. *Left* Column density, $N_{\rm H}$, is allowed to vary during the fit. The best-fit value is $N_{\rm H} = 1.217 \times 10^{20}$ cm^{-2}, which is more than an order of magnitude less than the value we would expect from the optical extinction. *Right* $N_{\rm H}$ is fixed to 3.074×10^{21} cm^{-2}, which is the value we would expect from applying the relationship of (Bohlin et al. 1978) to the colour excess ($E(B-V) = 0.53$). This larger column density provides a very poor fit to the data at low energies

an estimated distance of 40.9 Mpc) that could be responsible for the ionisation. A more likely explanation is that the NLR around NGC 3147 is anisotropic, and our line of sight to the central black hole passes through a region of the NLR that is less dense.

NGC 3147 is an example of a class of galaxy often referred to as a 'true' Seyfert-2 (e.g. Ptak et al. 1996; Panessa and Bassani 2002; Georgantopoulos and Zezas 2003; Matt et al. 2012; Bianchi et al. 2008, 2012), which is a term used to describe a Seyfert nucleus that appears unobscured and in which no broad lines are detectable in the optical spectrum. In such cases, it is expected that the BLR must be missing as the absorption is insufficient to entirely obscure these lines. Nicastro et al. (2003) suggested a mechanism whereby the BLR is formed by accretion disc instabilities and showed how it may therefore disappear at accretion rates lower than $\dot{m}_{\rm E} \leq 10^{-3}$, a limit which is consistent with the low Eddington ratio of NGC 3147 ($\lambda = 2.811 \times 10^{-4}$). Contrary to this claim, however, I find many of the Palomar sources with broad emission lines (especially amongst the LINER population) have Eddington ratios well below the 10^{-3} limit (see Fig. 2.6), although it must be added that the detection of broad H α and H β lines in the spectra of the low accretion rate sources (Ho et al. 1997c) is likely to be subject to some considerable uncertainty.

Various alternative theories have been proposed to explain the lack of broad lines in NGC 3147. For instance, Matt et al. (2012) argue that the source could actually be Compton thick (despite the soft, power-law spectrum suggesting otherwise) if a highly ionised surface were responsible for the reflection. However, the authors' *Suzaku* observation of energies above 10 keV failed to find any convincing evidence of an obscured AGN. A more likely explanation for the lack of broad lines is possibly that NGC 3147 is completely face-on in terms of inclination (as suggested by Shi et al. (2010)), and the orbital motion which we would normally expect to broaden the emission lines is therefore perpendicular to our line of sight.

2.13 X-ray Luminosity, Radio Luminosity and the Fundamental Plane

The emission from AGN is distributed throughout the electromagnetic spectrum and, in order to understand the nature of LLAGN, it will be necessary to consider more than one waveband. The penetrating nature of radio emission, combined with the very high angular resolution that can be obtained, makes it particularly suitable for studying AGN. In XRB systems it is known that radio loudness increases at lower accretion rates as the source enters the hard state, which is indicative of the presence of jets launched by a geometrically thick, radiatively inefficient accretion flow (e.g. Meier 2001; Wu and Cao 2008). Merloni et al. (2003) found a relation between the black hole mass, the radio luminosity and the X-ray luminosity (known as the fundamental plane) such that $\log L_{\mathrm{R}} = (0.60^{+0.11}_{-0.11}) \log L_{\mathrm{X}} + (0.78^{+0.11}_{-0.09}) \log M_{\mathrm{BH}} + 7.33^{+4.05}_{-4.07}$. This relationship applies for both AGN and stellar mass black holes and could provide a powerful method of confirming the AGN nature of many LLAGN.

Figure 2.13 (top left) shows a plot of X-ray luminosity against radio luminosity, where the X-ray luminosity data are from my *Chandra* survey and the radio data are from the literature (the Palomar sources from Nagar et al. (2005) and the PG quasars from Kellermann et al. (1994)). The plot shows considerable scatter, with the Seyfert-1s clearly distinct from the LINERs. By fitting a fundamental plane to the data, and adjusting the x-axis accordingly, the scatter is reduced and the correlation becomes much tighter (see Fig. 2.13, top right). From my fits I find that $\log L_{\mathrm{R}} = 0.68 \log L_{2-10\,\mathrm{keV}} + 0.92 \log M_{\mathrm{BH}} + 3.34$, which compares favourably to the values found by Merloni et al. (2003). However, the same cannot be said of the fits to only the Palomar sources ($\log L_{\mathrm{R}} = 0.37 \log L_{2-10\,\mathrm{keV}} + 0.77 \log M_{\mathrm{BH}} + 16.57$) or the LINER sources ($\log L_{\mathrm{R}} = 0.48 \log L_{2-10\,\mathrm{keV}} + 0.77 \log M_{\mathrm{BH}} + 12.35$—see Fig. 2.13, bottom left and right). Unfortunately, very few of the H II regions or transitions regions have radio luminosities available in the literature (although, in the case of the former, very few are expected to have compact radio cores). If these data were available then the fundamental plane could potentially be used to verify whether or not the emission in these sources is of an AGN origin. For example, if the X-ray and radio emission were caused by a compact population of 1,000 X-ray binary systems in the vicinity of a $10^6\ M_{\odot}$ SMBH then the radio emission would be expected to be $\sim$2.7 orders of magnitude weaker than if the emission was from the SMBH itself. A source with these properties would be sufficiently offset from the fundamental plane correlation to be easily identifiable. The forthcoming LeMMINGs e-Merlin legacy survey will provide detailed radio observations of all Palomar objects above declination 20° and may help provide some answers concerning the nature of these sources.

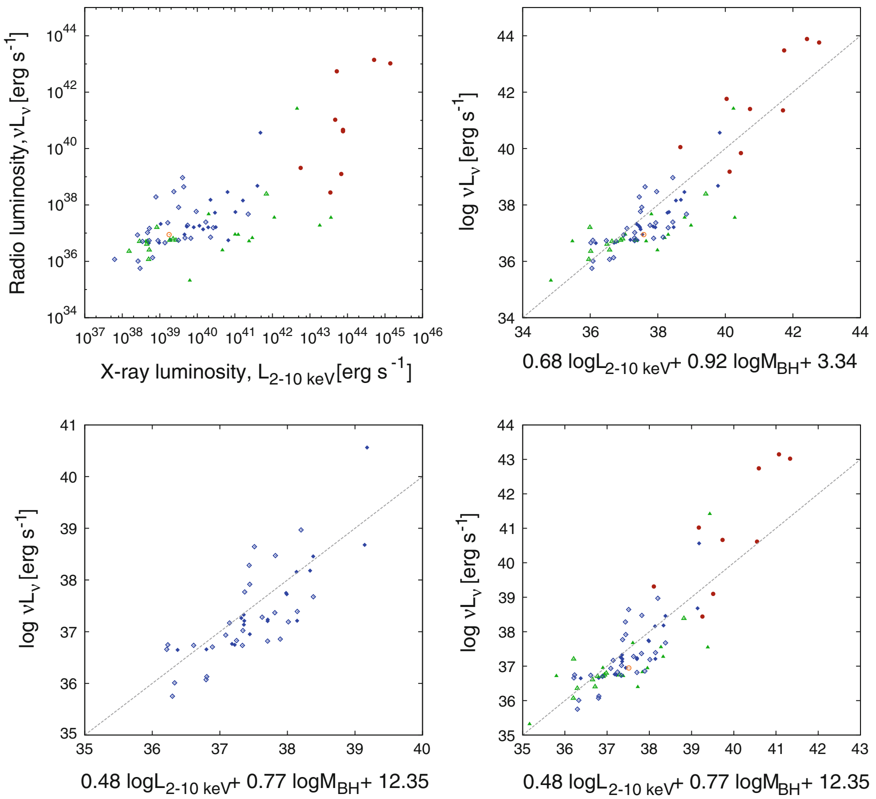

Fig. 2.13 *Top left* Plot of X-ray luminosity ($L_{2-10\ \mathrm{keV}}$) versus radio luminosity (νL_ν). *Top right* As before, except the X-ray luminosity has been corrected by fitting a fundamental plane to the data, such that $\log L_\mathrm{R} = 0.68 \log L_{2-10\ \mathrm{keV}} + 0.92 \log M_\mathrm{BH} + 3.34$. *Bottom left* Best fit to the fundamental plane from my LINER data. I find that $\log L_\mathrm{R} = 0.48 \log L_{2-10\ \mathrm{keV}} + 0.77 \log M_\mathrm{BH} + 12.35$. *Bottom right* The fundamental plane fitted to the LINER data is applied to the other sources as well, and appears to be an unsatisfactory fit to the quasars and the two radio-loud Palomar sources (NGC 315 and NGC 1275). In all plots the *filled* and *open blue diamonds* represent type-1.0–1.9 and type-2 LINERs respectively, filled and *open green diamonds* represent type-1.0–1.9 and type-2 Seyferts respectively, *red circle* represent the PG quasars and the *orange circles* represent the transition regions. X-ray data are from my *Chandra* survey, radio data for the Palomar sources are 15 GHz VLA observations (Nagar et al. 2005) and radio data for the PG quasars are 5 GHz VLA observations (Kellermann et al. 1994)

2.14 Summary of the Main Observational Results

- The 2–10 keV X-ray spectra of Palomar galaxies show no indication of Compton thickness amongst sources where the luminosity of the [O III] line satisfies $L_{[\mathrm{O\,III}]} \leq 10^{39}\ \mathrm{erg\,s^{-1}}$. At low luminosities the ionisation of the narrow line region may be dominated by stellar processes and the ratio of optical line strength to X-ray luminosity is probably unreliable as a Compton-thick indicator.

- Seyferts and LINERs with high X-ray to [O III] ratios show (by their $N_H/E(B-V)$ ratios) much higher absorption in the X-ray band than in the optical, indicating that the origin of the X-ray emission is deep within the AGN where the photons are subjected to much greater obscuration that that which affects the narrow line region further out. Seyferts/LINERs with low X-ray to [O III] ratios instead show $N_H/E(B-V)$ ratios which are consistent with absorption by the same material in both the X-ray and optical bands.
- The majority of type-2 Seyferts and LINERs in the sample have X-ray column densities of $\sim 10^{21}$ cm^{-2}, whereas type-1 Seyferts and LINERs have column densities that are distributed evenly over a large range ($<10^{24}$ cm^{-2}). The type-2 sources are therefore consistent with either a non-AGN origin or with scattering of intrinsic AGN emission from a reprocessor further out from the centre.
- H II region nuclei and LINERs all have Eddington ratios below $\sim$0.1 % of the Eddington limit, and show little or no overlap in black hole mass (with the LINERs occupying the high end of M_{BH}-space). Some LINERs with broad optical emission lines have Eddington ratios as low as 10^{-6}, which is not consistent with theories promoting the disappearance of the broad line region at low accretion rates.

2.15 Discussion

Low luminosity AGN remain a somewhat untidy, confusing and complex class of object, with no single model seemingly able to describe all the properties in an entirely consistent way. For instance, there's no doubt that the unified model of Antonucci and Miller (1985) successfully explains the presence of polarised broad lines in many sources by invoking the dusty torus but, equally, it's also clear that there are just as many type-2 sources to which this model does not apply. The major difficulty that is encountered when studying low accretion rate sources is that the luminosity of the AGN no longer greatly exceeds that of the other sources expected to exist within the host galaxy, and contamination is therefore a problem at all wavelengths. Even the sub-arcsecond angular resolution of *Chandra* does not necessarily isolate the emission related to the accretion flow. LLAGN may therefore be fairly diverse in nature and, in order to compare these sources to Galactic X-ray binary systems, it is likely that careful selection of the sample will be more effective than attempting to model all the different spectral classifications of LLAGN.

Possibly the most important progression towards an understanding of LLAGN would be to reliably identify the Compton-thick candidates. In this chapter I have shown that the use of the [O III]$_{5007\lambda}$ emission line as an indicator of intrinsic X-ray luminosity is unreliable at low luminosities and, in fact, there is little evidence for Compton thickness amongst any source where $L_{[O\,III]} \leq 10^{39}$ erg s^{-1}. Instead, at these low luminosities the ionisation of the narrow line region may be dominated by stellar processes, and the discovery of a compact and massive stellar cluster co-existing with the AGN in the inner few parsecs of the transition region galaxy NGC 4303 (Colina and Gonzalez Delgado 2002; Jiménez-Bailón et al. 2003) raises the possibility that nuclear star formation occurring on scales comparable to the torus may be common.

One thing that is clear, however, is that the detection of broad optical lines implies the presence of an AGN and broad-line sources generally show a tight correlation when their X-ray luminosity is plotted against properties such [O III] luminosity, radio luminosity or H α luminosity. It seems reasonable to expect that studies which are restricted to only type-1 Seyferts and LINERs are likely to find more similarities in behaviour with XRBs than studies which include all spectral types, and the presence of broad lines in some LINER sources at Eddington ratios as low as 10^{-6} means that such a restriction would have little effect on the range of accretion rates surveyed.

References

Antonucci, R. R. J., & Miller, J. S. (1985). Spectropolarimetry and the nature of NGC 1068. *Astrophysical Journal*, *297*, 621–632.

Baldwin, J. A., Phillips, M. M., & Terlevich, R. (1981). Classification parameters for the emission-line spectra of extragalactic objects. *Publications of the Astronomical Society of the Pacific*, *93*, 5–19.

Bassani, L., Dadina, M., Maiolino, R., Salvati, M., Risaliti, G., della Ceca, R., et al. (1999). A three-dimensional diagnostic diagram for Seyfert 2 galaxies: probing X-ray absorption and Compton thickness. *Astrophysical Journal Supplement*, *121*, 473–482.

Baumgartner, W. H., Tueller, J., Markwardt, C. B., Skinner, G. K., Barthelmy, S., Mushotzky, R. F., et al. (2012). The 70 Month swift-BAT all-sky hard X-ray survey. ArXiv e-prints.

Bianchi, S., Corral, A., Panessa, F., Barcons, X., Matt, G., Bassani, L., et al. (2008). NGC 3147: a 'true' type 2 Seyfert galaxy without the broad-line region. In L. Lanteri, C. M. Raiteri, A. Capetti, and P. Rossi, (Eds.), 8th National Conference on AGN.

Bianchi, S., Panessa, F., Barcons, X., Carrera, F. J., La Franca, F., Matt, G., et al. (2012). Simultaneous X-ray and optical observations of true type 2 Seyfert galaxies. *Monthly Notices of the Royal Astronomical Society*, *426*, 3225–3240.

Blackburn, J. K. (1995). FTOOLS: a FITS data processing and analysis software package. In R. A. Shaw, H. E. Payne, and J. J. E. Hayes, (Eds.), Astronomical Data Analysis Software and Systems IV, volume 77 of ASP Conference Series, p. 367.

Bohlin, R. C., Savage, B. D., & Drake, J. F. (1978). A survey of interstellar H I from L-alpha absorption measurements II. *Astrophysical Journal*, *224*, 132–142.

Brightman, M., & Nandra, K. (2008). On the nature of unabsorbed Seyfert 2 galaxies. *Monthly Notices of the Royal Astronomical Society*, *390*, 1241–1249.

Cappi, M. (2006). Relativistic blue- and red-shifted absorption lines in AGNs. *Astronomische Nachrichten*, *327*, 1012.

Cardelli, J. A., Clayton, G. C., & Mathis, J. S. (1989). The relationship between infrared, optical, and ultraviolet extinction. *Astrophysical Journal*, *345*, 245–256.

Cid Fernandes, R., Schlickmann, M., Stasinska, G., Asari, N. V., Gomes, J. M., Schoenell, W., Mateus, A., & Sodré, Jr., L. (2009). The Starburst-AGN disconnection: LINERs as retired galaxies. In W. Wang, Z. Yang, Z. Luo, and Z. Chen, (Eds.), The Starburst-AGN Connection, volume 408 of Astronomical Society of the Pacific Conference Series, p. 122.

Colina, L., Gonzalez Delgado, R., Mas-Hesse, J. M., & Leitherer, C. (2002). Detection of a super-star cluster as the ionizing source in the low-luminosity active galactic nucleus NGC 4303. *Astrophysical Journal*, *579*, 545–553.

Constantin, A., Green, P., Aldcroft, T., Kim, D.-W., Haggard, D., & Barkhouse, W. (2009). Probing the balance of AGN and star-forming activity in the local universe with ChaMP. *Astrophysical Journal*, *705*, 1336–1355.

Della Ceca, R., Severgnini, P., Caccianiga, A., Comastri, A., Gilli, R., Fiore, F., et al. (2008). Heavily obscured AGN with BeppoSAX, INTEGRAL, SWIFT, XMM and Chandra: prospects for Simbol-X. *Memorie della Societa Astronomica Italiana*, *79*, 65.

Georgantopoulos, I., & Akylas, A. (2010). Comparison between the luminosity functions of X-ray and [OIII] selected AGN. *Astronomy and Astrophysics*, *509*, A38.

Georgantopoulos, I., Rovilos, E., Akylas, A., Comastri, A., Ranalli, P., Vignali, C., et al. (2011). On the L_x–L_{6m} ratio as a diagnostic for Compton-thick AGN. *Astronomy and Astrophysics*, *534*, A23.

Georgantopoulos, I., & Zezas, A. (2003). Chandra observations of NGC 4698: A Seyfert 2 galaxy with no absorption. *Astrophysical Journal*, *594*, 704–708.

González-Martín, O., Masegosa, J., Márquez, I., & Guainazzi, M. (2009a). Fitting liner nuclei within the active galactic nucleus family: a matter of obscuration? *Astrophysical Journal*, *704*, 1570–1585.

González-Martín, O., Masegosa, J., Márquez, I., Guainazzi, M., & Jiménez-Bailón, E. (2009b). An X-ray view of 82 LINERs with Chandra and XMM-Newton data. *Astronomy and Astrophysics*, *506*, 1107–1121.

González-Martín, O., Papadakis, I., Braito, V., Masegosa, J., Márquez, I., Mateos, S., et al. (2011). Suzaku observation of the LINER NGC 4102. *Astronomy and Astrophysics*, *527*, A142.

Ho, L. C., Feigelson, E. D., Townsley, L. K., Sambruna, R. M., Garmire, G. P., Brandt, W. N., et al. (2001). Detection of nuclear X-ray sources in nearby galaxies with chandra. *Astrophysical Journal Letters*, *549*, L51–L54.

Ho, L. C., Filippenko, A. V., & Sargent, W. L. W. (1997a). A Search for "Dwarf" Seyfert nuclei. III. spectroscopic parameters and properties of the host galaxies. *Astrophysical Journal Supplement*, *112*, 315.

Ho, L. C., Filippenko, A. V., & Sargent, W. L. W. (1997b). A search for "Dwarf" Seyfert nuclei. V. demographics of Nuclear activity in nearby galaxies. *Astrophysical Journal*, *487*, 568.

Ho, L. C., Filippenko, A. V., Sargent, W. L. W., & Peng, C. Y. (1997c). A Search for "Dwarf" Seyfert Nuclei. IV. Nuclei with Broad H alpha Emission. *Astrophysical Journal Supplement*, *112*, 391.

Ho, L. C., Greene, J. E., Filippenko, A. V., & Sargent, W. L. W. (2009). A search for "Dwarf" Seyfert nuclei. VII. A catalog of central stellar velocity dispersions of nearby galaxies. *Astrophysical Journal Supplement*, *183*, 1–16.

Hopkins, P. F., Hickox, R., Quataert, E., & Hernquist, L. (2009). Are most low-luminosity active galactic nuclei really obscured? *Monthly Notices of the Royal Astronomical Society*, *398*, 333–349.

Inoue, H., Terashima, Y., & Ho, L. C. (2007). Fe K line profile in low-redshift quasars: average shape and eddington ratio dependence. *Astrophysical Journal*, *662*, 860–871.

Iyomoto, N., Fukazawa, Y., Nakai, N., & Ishihara, Y. (2001). BeppoSAX observation of NGC 3079. *Astrophysical Journal Letters*, *561*, L69–L72.

Jiménez-Bailón, E., Santos-Lleó, M., Mas-Hesse, J. M., Guainazzi, M., Colina, L., Cerviño, M., et al. (2003). Nuclear activity and massive star formation in the low-luminosity active galactic nucleus NGC 4303: Chandra X-ray observations. *Astrophysical Journal*, *593*, 127–141.

Kellermann, K. I., Sramek, R. A., Schmidt, M., Green, R. F., & Shaffer, D. B. (1994). The radio structure of radio loud and radio quiet quasars in the palomar bright quasar survey. *Astrophysical Journal*, *108*, 1163–1177.

Kewley, L. J., Groves, B., Kauffmann, G., & Heckman, T. (2006). The host galaxies and classification of active galactic nuclei. *Monthly Notices of the Royal Astronomical Society*, *372*, 961–976.

Maiolino, R., Salvati, M., Bassani, L., Dadina, M., della Ceca, R., Matt, G., et al. (1998). Heavy obscuration in X-ray weak AGNs. *Astronomy and Astrophysics*, *338*, 781–794.

Marconi, A., Risaliti, G., Gilli, R., Hunt, L. K., Maiolino, R., & Salvati, M. (2004). Local supermassive black holes, relics of active galactic nuclei and the X-ray background. *Monthly Notices of the Royal Astronomical Society*, *351*, 169–185.

Matt, G., Bianchi, S., Guainazzi, M., Barcons, X., & Panessa, F. (2012). The Suzaku X-ray spectrum of NGC 3147. Further insights on the best “true” Seyfert 2 galaxy candidate. 2012. *Astronomy and Astrophysics*, *540*, A111.

Meier, D. L. (2001). The association of jet production with geometrically thick accretion flows and black hole rotation. *Astrophysical Journal Letters*, *548*, L9–L12.

Merloni, A., Heinz, S., & di Matteo, T. (2003). A fundamental plane of black hole activity. *Monthly Notices of the Royal Astronomical Society*, *345*, 1057–1076.

Nagar, N. M., Falcke, H., & Wilson, A. S. (2005). Radio sources in low-luminosity active galactic nuclei. IV. Radio luminosity function, importance of jet power, and radio properties of the complete Palomar sample. *Astronomy and Astrophysics*, *435*, 521–543.

Narayan, R., Mahadevan, R., & Quataert, E. (1998). Advection-dominated accretion around black holess. In M. A. Abramowicz, G. Bjornsson, and J. E. Pringle, (Eds.), Theory of Black Hole Accretion Disks, p. 148.

Narayan, R., & McClintock, J. E. (2008). Advection-dominated accretion and the black hole event horizon. *New Astronomy Review*, *51*, 733–751.

Nicastro, F., Martocchia, A., & Matt, G. (2003). The lack of broad-Line regions in low accretion rate active galactic nuclei as evidence of their origin in the accretion disk. *Astrophysical Journal Letters*, *589*, L13–L16.

Osterbrock, D. E. (1977). Spectrophotometry of Seyfert 1 galaxies. *Astrophysical Journal*, *215*, 733–745.

Panessa, F., & Bassani, L. (2002). Unabsorbed Seyfert 2 galaxies. *Astronomy and Astrophysics*, *394*, 435–442.

Panessa, F., Bassani, L., Cappi, M., Dadina, M., Barcons, X., Carrera, F. J., et al. (2006). On the X-ray, optical emission line and black hole mass properties of local Seyfert galaxies. *Astronomy and Astrophysics*, *455*, 173–185.

Pappa, A., Georgantopoulos, I., Stewart, G. C., & Zezas, A. L. (2001). The X-ray spectra of optically selected Seyfert 2 galaxies: are there any Seyfert 2 galaxies with no absorption? *Monthly Notices of the Royal Astronomical Society*, *326*, 995–1006.

Predehl, P., & Schmitt, J. H. M. M. (1995). X-raying the interstellar medium: ROSAT observations of dust scattering halos. *Astronomy and Astrophysics*, *293*, 889–905.

Ptak, A., Yaqoob, T., Serlemitsos, P. J., Kunieda, H., & Terashima, Y. (1996). The nature of the low-luminosity active galactic nuclei in NGC 3147. *Astrophysical Journal*, *459*, 542.

Quataert, E. (2001). Low radiative-efficiency accretion flows. In B. M. Peterson, R. W. Pogge, and R. S. Polidan, (Eds.), Probing the Physics of Active Galactic Nuclei, volume 224 of Astronomical Society of the Pacific Conference Series, p. 71.

Richings, A. J., Uttley, P., & Körding, E. (2011). The connection between radio loudness and central surface brightness profiles in optically selected low-luminosity active galaxies. *Monthly Notices of the Royal Astronomical Society*, *415*, 2158–2172.

Shi, Y., Rieke, G. H., Smith, P., Rigby, J., Hines, D., Donley, J., et al. (2010). Unobscured type 2 active galactic nuclei. *Astrophysical Journal*, *714*, 115–129.

Taniguchi, Y., Shioya, Y., & Murayama, T. (2000). Post-starburst Models of LINERS. *Astronomical Journal*, *120*, 1265–1272.

Terashima, Y., Ho, L. C., & Ptak, A. F. (2000). Hard X-ray emission and the ionizing source in LINERS. *Astrophysical Journal*, *539*, 161–165.

Tran, H. D. (2001). Hidden broad-line Seyfert 2 galaxies in the CFA and 12 μM Samples. *Astrophysical Journal Letters*, *554*, L19–L23.

Tremaine, S., Gebhardt, K., Bender, R., Bower, G., Dressler, A., Faber, S. M., et al. (2002). The Slope of the black hole mass versus velocity dispersion correlation. *Astrophysical Journal*, *574*, 740–753.

Wu, Q., & Cao, X. (2008). Jet power extracted from ADAF and the applications to X-ray binaries and the radio galaxy FR dichotomy. *Astrophysical Journal*, *687*, 156–161.

Younes, G., Porquet, D., Sabra, B., & Reeves, J. N. (2011). Study of LINER sources with broad Hα emission. X-ray properties and comparison to luminous AGN and X-ray binaries. *Astronomy and Astrophysics*, *530*, A149.

Zhang, J. S., Henkel, C., Kadler, M., Greenhill, L. J., Nagar, N., Wilson, A. S., et al. (2006). Extragalactic H_2O masers and X-ray absorbing column densities. *Astronomy and Astrophysics*, *450*, 933–944.

Springer

http://www.springer.com/978-3-319-09586-8

Fast Spectral Variability in the X-ray Emission of Accreting Black Holes
Skipper, C.
2015, XXXIII, 150 p. 79 illus., 64 illus. in color., Hardcover
ISBN: 978-3-319-09586-8